Single-molecule dynamics of phytochrome-bound fluorophores probed by fluorescence correlation spectroscopy

Abigail E. Miller*†, Amanda J. Fischer‡, Ted Laurence†, Christopher W. Hollars†§, Richard J. Saykally*, J. Clark Lagarias‡¶, and Thomas Huser†§‖

*Department of Chemistry, University of California, Berkeley, CA 94720; ‡Section of Molecular and Cellular Biology, University of California, Davis, CA 95616; †Chemistry and Materials Science Directorate, Lawrence Livermore National Laboratory, Livermore, CA 94550; and §National Science Foundation Center for Biophotonics Science and Technology, Sacramento, CA 95817

Contributed by J. Clark Lagarias, June 6, 2006

Fluorescence correlation spectroscopy (FCS) was used to investigate the hydrodynamic and photophysical properties of PR1 (phytofluor red 1), an intensely red fluorescent biliprotein variant of the truncated cyanobacterial phytochrome 1 (Cph1Δ, which consists of the N-terminal 514 amino acids). Single-molecule diffusion measurements showed that PR1 has excellent fluorescence properties at the single-molecule level, making it an interesting candidate for red fluorescent protein fusions. FCS measurements for probing dimer formation in solution over a range of protein concentrations were enabled by addition of Cph1Δ apoprotein (apoCph1Δ) to nanomolar solutions of PR1. FCS brightness analysis showed that heterodimerization of PR1 with apoCph1Δ altered the chemical environment of the PR1 chromophore to further enhance its fluorescence emission. Fluorescence correlation measurements also revealed interactions between apoCph1Δ and the red fluorescent dyes Cy5.18 and Atto 655 but not Alexa Fluor 660. The concentration dependence of protein:dye complex formation indicated that Atto 655 interacted with, or influenced the formation of, the apoCph1 dimer. These studies presage the utility of phytofluor tags for probing single-molecule dynamics in living cells in which the fluorescence signal can be controlled by the addition of various chromophores that have different structures and photophysical properties, thereby imparting different types of information, such as dimer formation or the presence of open binding faces on a protein.

biliprotein photoreceptor | phytofluor | single-molecule fluorescence | biophotonics

Phytochromes are biliprotein photosensors that regulate many physiological processes in green plants, enabling their adaptation to fluctuating light environments (1, 2). Phytochrome-related proteins also function as regulators of a diverse array of physiological processes in microorganisms, including many nonphotosynthetic species (3, 4). Phytochromes are large proteins with covalently bound linear tetrapyrrole (bilin) chromophores that transduce light signals by means of their ability to reversibly photointerconvert between red-light-absorbing (P_r) and far-red-light-absorbing (P_{fr}) species, a process that typically initiates a transcriptional signaling cascade (5–8). The excited-state lifetimes of phytochromes are quite short (i.e., <20 ps) because of the photochemical deexcitation of their bilin chromophores by means of efficient double-bond isomerization (9). For this reason, phytochromes are poorly fluorescent biliproteins, a property that distinguishes this family of photoreceptors from the intensely fluorescent phycobiliproteins found in cyanobacteria and red algae (10).

Our current understanding of the photophysics of bilins bound within a phytochrome apoprotein scaffold has greatly benefited from studies in which the structures of both bilin chromophores and apoproteins have been modified. By introduction of bilin analogs that lack the photoisomerizing double bond, intensely yellow-orange fluorescent holoproteins (also known as phytofluors) have been produced (11). Directed evolution of a truncated cyanobacterial phytochrome (Cph1Δ, consisting of the N-terminal 514 amino acids) yielded a mutant apoprotein that binds the native chromophore precursor, phycocyanobilin (PCB), to produce the red-emitting PR1 (phytofluor red 1) (12). Mutation of a conserved tyrosine residue was responsible for this fluorescence enhancement, and other amino acid substitutions for this tyrosine produced previously uncharacterized phytochrome holoproteins with altered photophysical properties (13). The observation that one of the Cph1Δ mutants apparently has enhanced affinity for porphyrins indicates that phytochrome's ligand-binding specificity also can be tuned by mutagenesis (13).

The ability to tag proteins of interest through fusion with an apophytochrome gene and to produce phytofluors within living cells has compelled us to investigate the single-molecule fluorescence properties of this class of genetically encoded fluorescent proteins. The ability to generate yellow-orange phytofluors in living cells has already been exploited to distinguish two populations of phytochrome molecules in the moss *Ceratodon purpureus* by fluorescence correlation spectroscopy (FCS) (14). The present study was undertaken to examine the single-molecule hydrodynamics of the red-emitting phytofluor PR1 and its WT parent, Cph1Δ, by using FCS (15, 16). These studies not only document the feasibility of this technique for probing the affinity of the two subunits within the phytochrome dimer but also unexpectedly reveal the striking affinity of the Cph1Δ apoprotein (apoCph1Δ) for organic fluorophore dyes measured at the single-molecule level.

Results and Discussion

The Brightly Fluorescent Cph1Δ Mutant PR1 Enables Single-Molecule Fluorescence Detection. FCS was performed on the red fluorescent Cph1 mutant PR1 containing the Tyr-176-His substitution. PR1 has the same domain structure as Cph1Δ, a truncated version of the full-length Cph1 photoreceptor that lacks the histidine kinase regulatory domain (Fig. 1*A*). It is well established that removal of the histidine kinase domain does not affect chromophore attachment or alter the spectroscopic properties of the full-length Cph1 photoreceptor (17–19). As shown in Fig. 1*B*,

Conflict of interest statement: No conflicts declared.

Abbreviations: Cph1Δ, truncated cyanobacterial phytochrome 1; apoCph1Δ, Cph1Δ apoprotein; FCS, fluorescence correlation spectroscopy; PR1, phytofluor red 1; PCB, phycocyanobilin; P_{fr}, far-red-light-absorbing phytochrome.

¶To whom correspondence may be addressed at: Section of Molecular and Cellular Biology, College of Biological Sciences, University of California, One Shields Avenue, Davis, CA 95616. E-mail: jclagarias@ucdavis.edu.

‖To whom correspondence may be addressed at: National Science Foundation Center for Biophotonics, 2700 Stockton Boulevard, Suite 1400, Sacramento, CA 95817. E-mail: trhuser@ucdavis.edu.

www.pnas.org/cgi/doi/10.1073/pnas.0604724103

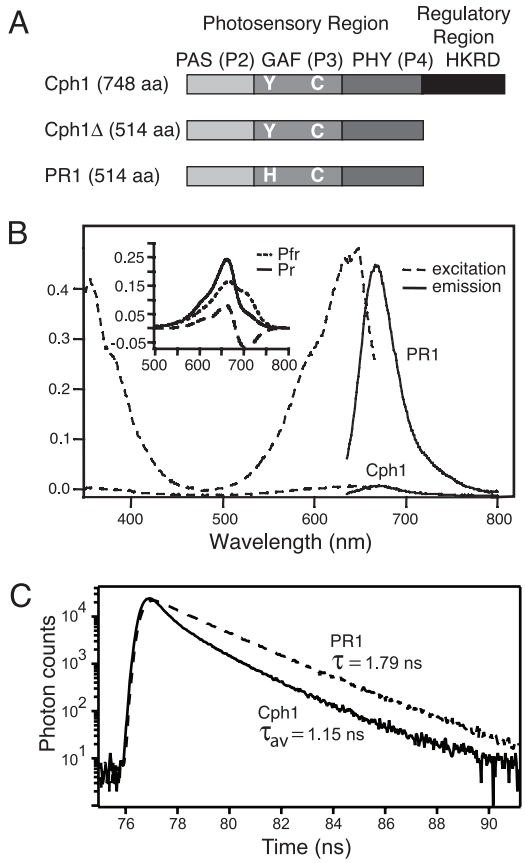

Fig. 1. Comparative structural and spectroscopic properties of the wild type and PR1 mutant of Cph1Δ. (*A*) Domain architecture of the cyanobacterial phytochrome 1 (Cph1), the Cph1Δ deletion mutant, and the red fluorescent mutant PR1. PCB is covalently linked to conserved cysteine 259 (indicated by ''C''). PR1 has the same primary structure as Cph1Δ, with the exception of the substitution of a histidine for tyrosine at position 176 (indicated by ''H'' and ''Y,'' respectively). (*B*) Raw excitation and emission spectra of Cph1Δ and PR1. (*Inset*) Absorption spectra of the red-light-absorbing P_r form (solid line) and the far-red-light-absorbing P_{fr} form (dashed line) of WT Cph1Δ after saturating far-red and red irradiation, respectively. The third curve (dashed line) is the difference in the absorption of the red and the far-red forms. (*C*) Fluorescence lifetime of WT Cph1Δ (solid line) and the mutant PR1 (dashed line) as measured by time-correlated single-photon counting with ≈80-ps-long excitation pulses at 640 nm.

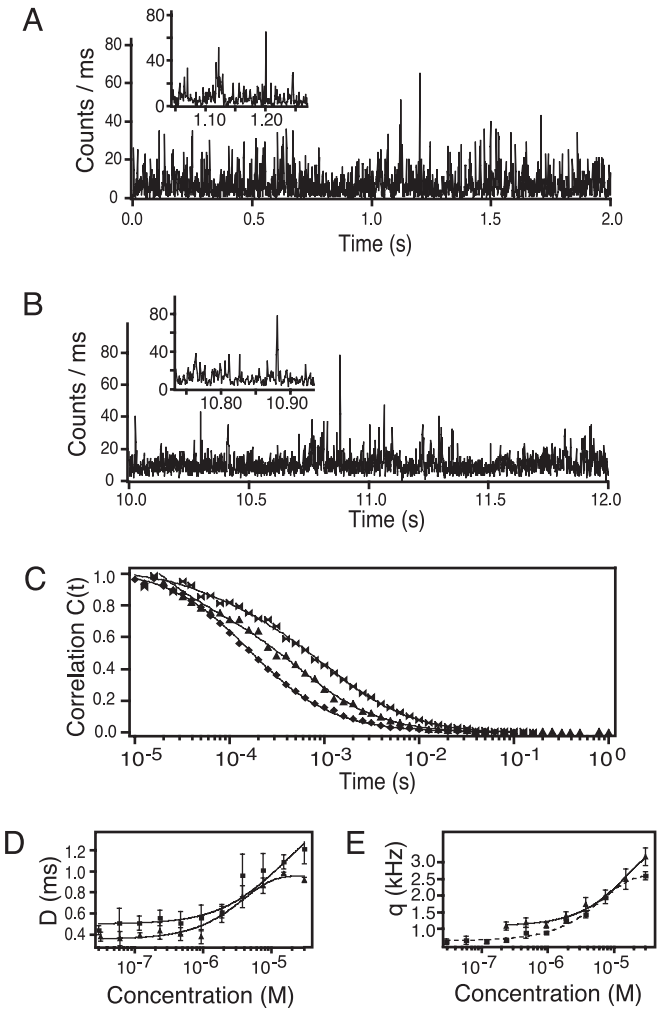

Fig. 2. Fluorescence correlation spectroscopic analysis of PR1. (*A*) Intensity transient of a solution of 100 pM of the red fluorescent dye Atto 655 displayed with 1-ms bin width. (*B*) Intensity transient of 1 nM PR1 mixed with 30 μM apoCph1Δ. Both fluorophores were excited by a 640-nm diode laser at 150-μW power focused to a diffraction-limited spot in solution. (*A Inset* and *B Inset*) Discrete photon bursts indicate fluorescence from single molecules. (*C*) Fluorescence correlation plots. Data from the 100 pM Atto 655 solution are shown as circles. A fit results in a diffusion time of 140 μs for Atto 655. Also shown are fluorescence correlation plots of 1.5 nM PR1 in the presence of a low concentration of apoCph1Δ (10^{-8} M) (triangles) and a high concentration of apoCph1Δ (10^{-6} M) (dumbbells). The shift in diffusion time at high protein concentration indicates protein–protein interactions. (*D*) Diffusion time of PR1 plotted as a function of the total Cph1Δ concentration for two independent measurements. The concentration of the fluorescent mutant PR1 was kept constant at 1 nM; the concentrations of the nonfluorescent apoproteins, apoCph1Δ (squares) or apoPR1 (triangles), were varied over four orders of magnitude. (*E*) Chromophore brightness *q* as a function of protein concentration. Each data point in *D* and *E* reflects the average of six separate measurements.

the PR1 mutant is considerably more fluorescent than WT Cph1Δ, which has its main peak at 635 nm, whereas the fluorescence spectrum for PR1 is most intense at 670 nm (12, 13). This increase in fluorescence is primarily due to PR1's poor photointerconversion to the far-red-light-absorbing P_{fr} form (shown for WT Cph1Δ in Fig. 1*B Inset*; ref. 12). The increased fluorescence of PR1 compared with WT Cph1Δ is paralleled by an increase in fluorescence lifetime measured by histogramming photon emission by using single-photon detection (Fig. 1*C*). With this system, the fluorescence decay of WT Cph1Δ required fitting with two exponentials, resulting in an average lifetime of 1.15 ns. The two components have a primary decay time of 0.74 ns and a minor decay time of 2.2 ns. PR1, on the other hand, exhibited a single lifetime of 1.79 ns. These differences in fluorescence lifetimes correspond reasonably well with the differences in quantum yield of Cph1Δ and PR1 but also suggest further investigation beyond the scope of this contribution. The spectral properties of phytofluors are significantly red-shifted compared with the intrinsic absorption and fluorescence of other proteins and make PR1 a potentially interesting candidate for a fluorescent fusion protein for *in vivo* fluorescence studies.

At a solution concentration of 1 nM, where the average number of fluorophores present in the focal volume of the laser beam is near unity, their diffusion through the laser focus resulted in short, intense photon bursts. Fig. 2*A* shows a typical fluorescence intensity transient of a solution containing a 100 pM concentration of the red fluorescent dye Atto 655 (Atto-Tec, Siegen, Germany), used to calibrate the detection volume of our confocal microscope. With high temporal resolution, we could resolve the presence of distinct photon bursts, which correspond to the diffusion of single Atto 655 dye molecules through the

confocal detection spot (see Fig. 2*A Inset*). Fig. 2*B* shows similar data for a 1 nM solution of PR1 in the presence of 30 μM apoCph1Δ. As shown in the next paragraphs, mixing of the phytofluors with nonfluorescent apoproteins stabilizes the protein conformation and enables their detection at the single-molecule level, but it also adds noise in the form of increased Rayleigh and Raman scattering as well as weak autofluorescence to the intensity transients. Fig. 2*B Inset* again shows well separated photon bursts, indicating diffusion of individual phytochrome molecules through the focal volume. Both transients were obtained with the same laser excitation power of 150 μW at 632.8 nm. By comparing the intensity transients in Fig. 2*A* and *B*, it is apparent that there are more fluorescence bursts in the Atto 655 transient that are of higher intensity above the background than those of PR1. This increase is due to the higher fluorescence quantum yield of Atto 655 (0.3 compared with 0.15 for PR1) as well as the dark-state conversion of PR1 to the far-red form that must be accounted for when analyzing the fluorescence decay curves. The PR1 intensity trace also shows higher background levels due to the presence of the apoprotein at micromolar concentration.

Fig. 2*C* shows the result of a correlation analysis of time traces such as the ones in Fig. 2 *A* and *B*. There is approximately a one order of magnitude change in the diffusion time between Atto 655 (molecular mass of ≈500 Da) and the larger PR1 protein (molecular mass of 61,261 Da), a difference that results in a shift to longer diffusion times. A fit to the correlation plot for Atto 655 reveals an average diffusion time of 140 ± 5 μs, whereas the diffusion time for the PR1 monomer is 450 ± 60 μs. The shape of the Cph1 correlation function also exhibits a less sharp S curve dependence, indicating the contribution of phototransformation to the far-red dark state (see Fig. 2*C*).

PR1 Forms Dimers with apoCph1Δ in the Micromolar Concentration Range. FCS can also be used to study molecular interactions at low concentrations. The diffusion time τ_D of a molecule, when modeled as a noninteracting, uncharged spherical particle, is proportional to the solution viscosity η, the particle diameter d, and the square of the beam-waist ω_0 at the focus of the laser beam (15, 16). The diffusion time is also inversely proportional to the solution temperature T.

$$\tau_D = \frac{\omega_0^2 3\eta\pi d}{4kT} \quad [1]$$

If the molecule under study interacts with other molecules, the main parameter that changes is the particle diameter, which will lead to an increase in diffusion time. Monitoring this change in diffusion time over a range of protein concentrations can be used to analyze protein–protein interactions. This analysis is further aided by the fact that, at typical protein equilibrium concentrations, the solution viscosity, which could also have an effect on τ_D, will not change significantly. A particular problem, however, is that FCS has a relatively narrow dynamic range (i.e., it performs well only in a concentration range of $\approx 10^{-8}$ to 10^{-11} M for the fluorescent probe). At lower concentrations, it takes a very long time to obtain a sufficient number of photon bursts to perform the autocorrelation analysis, whereas at higher concentrations, photon bursts can no longer be resolved. Fortunately, in the absence of its PCB chromophore, apoCph1Δ is essentially nonfluorescent, which allowed us to conduct interaction studies over a wide range of protein concentrations where the fraction of chromophore-containing PR1 protein is kept constant at 1 nM concentration. In Fig. 2*C*, we have also plotted correlation curves for PR1 in the presence of low (10^{-8} M) and high (10^{-6} M) concentrations of apoCph1Δ. These results show that micromolar apoCph1Δ concentrations led to a shift to longer diffusion times in the correlation curve for PR1. Similar results were observed when apoCph1Δ was replaced with apoPR1 (Fig. 2*D*). Such measurements indicate that the increase in diffusion time corresponds to specific interactions between PR1 and the apoproteins apoCph1Δ or apoPR1.

The PR1 diffusion time as a function of the total protein concentration is depicted in Fig. 2*D*. Here, each data point is the result of six independent FCS experiments for each apoprotein concentration. These measurements show that both apoproteins begin to interact with PR1 at concentrations of ≈1 μM, with interactions appearing to saturate at ≈30 μM. The onset of a saturation plateau at ≈20 μM is consistent with the formation of PR1:apoprotein heterodimers. Note that the concentration dependence of the increase in diffusion time is qualitatively very similar for the two apoproteins; the variation in the actual average diffusion time for the two experiments may reflect the slightly different experimental parameters on consecutive days (e.g., changes in the exact position of the laser focus with respect to the glass coverslip surface). Taken together, these results indicate that the binding affinities of both apoproteins for PR1 are similar. In support of this interpretation, the observed dimer dissociation constant is similar to the values of 10–50 μM that were recently reported for Cph1Δ (20).

Protein Dimerization Leads to an Increase in the Fluorescence Brightness of PR1. We have also studied the brightness, q, of PR1 as a function of Cph1Δ concentration. This parameter can be extracted from the fluorescence correlation data by covariance analysis. If the formation of dimers, as indicated by the increase in diffusion time, has no influence on the chromophore, then the brightness parameter should remain constant with increasing protein concentration. As shown in Fig. 2*E*, PR1 exhibits an increase in brightness with increasing Cph1Δ concentration. This increase in brightness correlates very well with the rise in the diffusion time of Cph1Δ (Fig. 2*D*). Note that even though PR1 is forming dimers at higher protein concentration, these dimers are formed with the nonfluorescent apoprotein, so each dimer still has only one chromophore. Because the PCB chromophore is covalently linked to Cph1Δ, we attribute this change in brightness to a stabilization of the bilin chromophore upon dimer formation. Free PCB (i.e., not bound to apoCph1Δ) has a fluorescence quantum yield that is a factor of 1,000 times lower than when it is bound to PR1 (13). This reduced quantum yield reflects the facile isomerization of PCB in solution. Binding to apoPR1 confers rigidity to the chromophore, thereby increasing its fluorescence quantum yield. The increase in brightness indicates that the formation of PR1:apoPR1 (or PR1:apoCph1Δ) dimers influences the chromophore-binding pocket (21). This increase in quantum yield could reflect reduced rates of nonradiative pathways or a reduced absorption coefficient.

apoCph1Δ Can Specifically Interact with Planar Aromatic Red Fluorescent Dye Ligands. We next used FCS measurements to determine whether apoCph1Δ can interact with the fluorescent dyes Cy5.18, Alexa Fluor 660, and Atto 655. All of these red-emitting fluorophores owe their fluorescence properties to an extended conjugated double-bond system, which provides for long-reaching electron delocalization. Cy5.18 belongs to the cyanine group of dyes and is the most conformationally flexible of the three dyes. Atto 655 is a member of the oxazine family of dyes, and Alexa Fluor 660 is a member of the rhodamine family of dyes.

To examine the interaction of the three dyes with Cph1Δ, 0.1 nM solutions of each dye were mixed with a wide range of apoCph1Δconcentrations. In the absence of protein, all dyes exhibited a diffusion time through the laser excitation spot of between 140 and 160 μs. As shown in Fig. 3, Alexa Fluor 660 exhibited no change in diffusion time with increasing concentrations of apoCph1Δ. Its behavior in the presence of apoCph1Δ

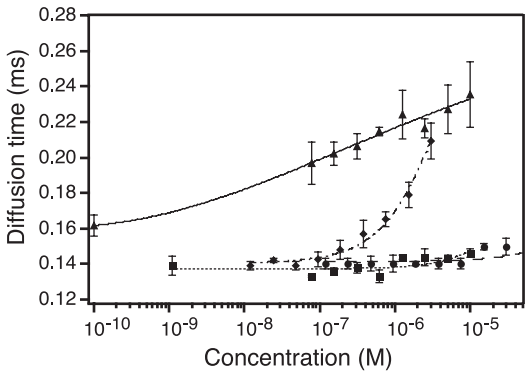

Fig. 3. Diffusion time of different red-emitting organic dyes as a function of protein concentration. The diffusion times of three different organic dyes (Cy5.18, triangles; Atto 655, diamonds; Alexa Fluor 660, squares) with their concentration fixed at 100 pM are shown as a function of Cph1Δ concentration. Also shown is the diffusion time of Atto 655 (circles) as a function of BSA concentration. The lines are guides to the eye. Each data point is the result of six separate measurements. Note that the native diffusion time of the fluorescent mutant PR1 is 500 μs.

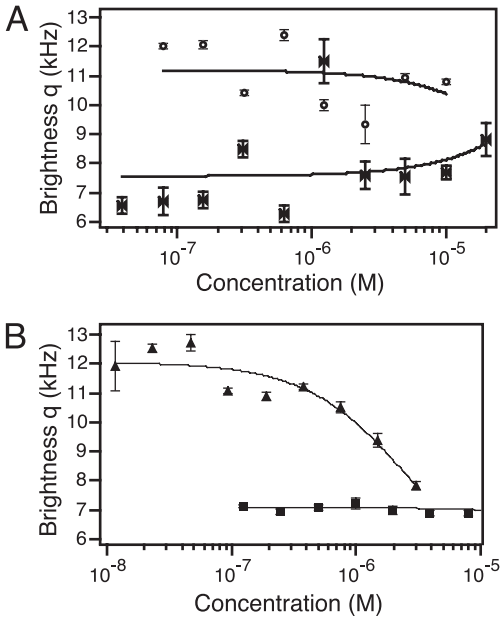

Fig. 4. Fluorescence brightness of organic dyes upon interaction with apoCph1Δ. (*A*) Fluorophore brightness for the dyes Alexa Fluor 660 (circles) and Cy5.18 (dumbbells) as a function of apoCph1Δ concentration. The dye concentration was fixed at 1 nM for Alexa Fluor 660 and 100 pM for Cy5.18. (*B*) Fluorophore brightness for the dye Atto 655 as a function of apoCph1 Δconcentration (triangles) and BSA concentration (squares). The Atto 655 concentration was fixed at 100 pM. Each data point in *A* and *B* is the result of six separate measurements. The different error bars for the brightness measurement of each fluorescent dye are due to their different photophysical properties (i.e., triplet-state blinking and quantum yield).

was very similar to the behavior of Atto 655 upon titration with BSA, which was used as a control (Fig. 3). These results indicate that Alexa Fluor 660 does not interact with apoCph1Δ, even at micromolar concentration. Surprisingly, both Cy5.18 and Atto 655 showed an increase in diffusion time when mixed with apoCph1Δ. The diffusion time of Atto 655 increased from 140 μs at nanomolar apoCph1Δ concentration to 200 μs in the presence of 3 μM apoCph1Δ (Fig. 3). Interestingly, the Atto 655 diffusion time increased biexponentially with apoCph1Δ, exhibiting no indication for any leveling off (Fig. 3). By comparison, Cy5.18 displayed a much more gradual dependence of its diffusion time on apoCph1Δ concentration. In both cases, the diffusion time never reached the diffusion time of the PR1 monomer at ≈500 μs. This finding indicates that the interactions of Atto 655 and Cy5.18 with apoCph1Δ are of sufficient duration to affect the diffusion rate of the dyes but are nonetheless transient. As revealed by the different rise in diffusion times, the nature of the transient interactions between the protein and Cy5.18 or Atto 655 appears to be different for the two dyes.

Cph1 Interactions with Atto 655 Lead to Fluorescence Quenching. As discussed above, we have also used a covariance analysis to obtain information about potential changes in brightness for the different fluorescent dyes upon interactions with apoCph1Δ. Fig. 4*A* shows the outcome of this analysis for Alexa Fluor 660 and Cy5.18. These measurements show that both dyes maintain their average brightness, even in the presence of micromolar concentrations of apoCph1Δ. This is not surprising for Alexa Fluor 660, because the diffusion analysis already indicated that it does not interact with Cph1. By comparison, Cy5.18 displayed an exponential dependence of its diffusion time on protein concentration, but the apoCph1Δ–Cy5.18 interaction does not influence its fluorescence brightness.

In contrast to the Cy5.18 and Alexa Fluor 660 dyes, Atto 655 displays an apparent exponential decrease in brightness with increasing concentrations of apoCph1Δ (see Fig. 4*B*). When mixed with BSA, however, there is no change in Atto 655's fluorescence brightness (Fig. 4*B*). Taken together, the changes in brightness and diffusion time indicate that the transient interaction between Atto 655 and apoCph1Δ leads to fluorescence quenching. This effect is most likely due to interactions with the bilin-binding pocket of apoCph1Δ. If Atto 655 was binding purely statically to apoCph1, its diffusion time would jump from 140 μs to ≈500 μs, the diffusion time observed for PR1 (see Fig. 2*C*). Tryptophan has been shown previously to be an efficient quencher for oxazine dyes (22, 23), which leads us to conclude that the decrease in brightness might be due to quenching of Atto 655 by one or more tryptophans on apoCph1Δ. Such fluorescence quenching reflects an efficient electron-transfer (ET) process from the dye to tryptophan, a process that is seen only for certain dyes (21, 22). Such ET, however, occurs only at very small dye–tryptophan separations (<1 nm), which again indicates, together with the change in diffusion time, that Atto 655 exhibits a high but transient affinity for apoCph1Δ.

It is tempting to speculate that Atto 655 binds to the same pocket in apoCph1Δ as that of the PCB prosthetic group; however, the concentration dependence of the interaction suggests that Atto 655 binds to an apoCph1Δ dimer. In this regard, the interactions between Atto 655 and Cph1 follow the same concentration dependence as dimerization of Cph1. Although it is possible that Atto 655 interacts with the bilin-binding pockets on both subunits, it is more likely that Atto 655 interacts at discrete sites on the apoCph1Δ homodimer. We note that there are seven tryptophans in Cph1Δ, only one of which lies within the GAF domain, where the natural bilin chromophore is bound. Based on the structure of the bacteriophytochrome drBphP (24), however, it is unlikely that this tryptophan (i.e., Trp-284) will be responsible for this electron-transfer quenching. Additional experiments will be needed to resolve the chemical nature of the Atto 655–apoCph1 interaction. It should also be noted that we did not observe any apparent effects of the interaction between the red fluorescent dyes and apoCph1 in bulk solution, a fact that we attribute to the transient nature of the interactions between the dyes and apoCph1, which can only be isolated and becomes apparent at the single-molecule level.

In summary, we have shown that the mutant of the light

sensory protein Cph1Δ, PR1, enables single-molecule detection of phytofluors. PR1 exhibits a marked increase in its fluorescence brightness upon dimerization, and apoCph1Δ can interact selectively with organic fluorescent dyes. This study has important implications for the use of phytofluors as fusion proteins for intracellular imaging. The combination of their brightness and pronounced red emission makes phytofluors potentially interesting reporters for single-molecule imaging and protein tracking applications in living cells. Unlike members of the GFP family (25), phytofluor production can be controlled externally through addition of the bilin chromophore, which should enable the long-term observation of intracellular events by means of the addition of low concentrations of chromophore precursors to regulate the rate of fluorophore formation. Also, the sensitivity of standard organic dyes to Cph1 complexes will have important implications for monitoring dimerization and phosphorylation of proteins in living cells. As is also seen by the recently demonstrated ability of phytochromes to act as light-controlled molecular switches for gene expression (26, 27), these proteins show great promise for a wide range of cell biology studies at the single-molecule level.

Materials and Methods

Fluorescent Dyes. Atto 655, Alexa Fluor 660 (Molecular Probes), and Cy5.18 (a gift from A. Waggoner, Carnegie Mellon University, Pittsburgh, PA) were dissolved in methanol to yield 1 mM stock solutions. All dyes were then diluted to micromolar to nanomolar concentrations by using 0.01 M PBS (0.138 M NaCl/0.0027 M KCl, pH 7.4).

Recombinant Phytochrome Expression and Purification. Apo- and holophytochromes were expressed in *Escherichia coli* strain LMG194 harboring *Synechocystis* sp. PCC 6803 WT Cph1Δ or PR1 mutant expression plasmids, pBAD-Cph1Δ or pBAD-PR1, in the presence (for holoprotein) or the absence (for apoprotein) of the PCB-producing plasmid pPL-PCB (17). Expression, purification, and concentration of the recombinant proteins were performed as described in ref. 12. Purified proteins were flash-frozen in liquid nitrogen and stored at −80°C in 25 mM Tes-KOH (pH 7.5) buffer containing 10% (vol/vol) glycerol. Protein concentrations were determined by absorbance at 280 nm, absorbance at 650 nm, and/or by absorbance difference spectroscopy (12).

Fluorescence Correlation and Lifetime Measurements. Dilute phytochrome samples were investigated by FCS by using a custom-built system based on an inverted optical microscope (Eclipse TE300; Nikon), which makes use of the 632.8-nm line of a helium–neon laser as the excitation source. The collimated laser beam is reflected into a ×100 oil immersion objective with a numerical aperture of 1.45 (Planapochromat; Zeiss) by using a dichromatic mirror (650DRLP; Omega Optical, Brattleboro, VT). The focus of the laser beam is translated ≈10 μm deep into solution, where it forms a tight spot of ≈1-μm^3 volume that is experimentally verified with a standard dye. Fluorescence is collected by the same microscope objective, passed through the dichromatic mirror, and focused through a confocal pinhole 150 μm in diameter. Fluorescent light is then recollimated, passed through a long-pass filter (655HQ; Chroma Technology, Rockingham, VT) to block residual light from the excitation laser, and split by a 50:50 beamsplitter (Newport, Irvine, CA). Each beam is then passed through a 700/90 band-pass filter (Chroma Technology) and focused directly onto a single-photon-counting avalanche photodiode (APD) (SPCM-AQR-14; PerkinElmer) by means of a 25-mm focal length planoconvex lens (Newport). Photon events were recorded with a timer-counter card (National Instruments, Austin, TX) that recorded the arrival time of each photon with 12.5-ns time resolution to the hard-disk drive of a personal computer system. Cross-correlation of recorded photon events from both APDs was performed by using a custom-written program in LABVIEW (National Instruments), and fits were performed in IGOR PRO (WaveMetrics, Lake Oswego, OR) (28). Cross-correlation was used to avoid false correlation events at short time scales from after-pulsing of the APDs. The fluorescence lifetime data were collected with the same FCS apparatus by using a pulsed diode laser (LDH640; PicoQuant, Berlin; 640-nm wavelength, 40-MHz repetition rate, and 80-ps pulse length) as the excitation source. The signal from the APDs was recorded as photon events by a TimeHarp 200 time-correlated single-photon-counting card (PicoQuant). Lifetime calculations were performed by using a custom-written program in LABVIEW, and fits were performed in IGOR PRO. Some lifetime calculations were also performed by the TimeHarp 200 software (PicoQuant) with data fit with FLUOFIT software (PicoQuant). System calibrations were performed by using the red-emitting dye Atto 655 as a reference.

FCS and fluorescence lifetime measurements for PR1 were conducted by using 100–300 pM and 3.3–330 nM protein concentrations, respectively. Various concentrations of apoCph1Δ or BSA (catalog no. A8531; Sigma-Aldrich) were added to the PR1 solutions as indicated. For each set of FCS measurements to study dye–apoCph1Δ interactions, the concentration of fluorescent dyes (Atto 655, Cy-5.18, or Alexa Fluor 660) was fixed between 0.1 and 1 nM while the overall protein concentration was varied by the addition of apoCph1Δ. A silicone rubber gasket (silicone isolator, 2-mm thickness, Sigma-Aldrich) was adhered to a clean glass coverslip (no. 1; Fisher Scientific) to provide a well in which 20 μl of sample solution was placed. For each concentration, six measurements were conducted consecutively, with each run lasting between 60 and 120 s.

FCS Analysis. Each solution was measured multiple times to obtain a statistical error distribution, which determines our accuracy in measuring diffusion times. For each run, the correlation function was calculated and then fit by using a 2D diffusion model (29) for the fluorescent dye Atto 655:

$$\langle G(\tau)\rangle = 1 + \frac{1}{N}\left(\frac{1}{\left(1+\frac{\tau}{\tau_D}\right)}\right). \qquad [2]$$

To account for the fluctuations of the PR1 between a fluorescent bright state and a dark state, an additional term is added to the diffusion model (30–32):

$$\langle G(\tau)\rangle = 1 + \frac{1}{N}\left(\frac{1}{\left(1+\frac{\tau}{\tau_D}\right)}\right)\left(1+\frac{T}{1-T}\exp\left(-\frac{\tau}{\tau_t}\right)\right). \qquad [3]$$

Here, τ is the delay time between the two photon burst transients, τ_D is the average diffusion time, N is the average number of fluorescent molecules in the focal volume, T is the fraction of fluorescent Cph1 molecules in the dark state, and τ_t is the dark-state conversion time. The dark-state term accounts for the conversion of Cph1 to the far-red (P_{fr}) absorbing state. Using a 2D diffusion model reduces the number of fit parameters needed, and the differences in the diffusion time between the two models (2D vs. 3D) are negligible (19). For each concentration, the diffusion time is determined from these fits and then averaged over multiple runs. The fluorescent dyes Atto 655, Alexa Fluor 660, and Cy5.18 show essentially no interconversion to a dark state; therefore, the simple 2D diffusion model was sufficient for determining their diffusion times.

Fluorescence Brightness Analysis. The brightness of PR1 as a function of concentration was determined by analyzing the covariance or nonnormalized correlation $\langle I(t)I(t+\tau)\rangle$ (33):

$$\mathrm{cov}(\tau_D) = \frac{cq^2}{\left(1 + \frac{\tau}{\tau_D}\right)}\left(1 + \frac{T}{1-T}\exp\left(-\frac{\tau}{\tau_t}\right)\right) + (k_{bkgd} + cq)^2. \quad [4]$$

Fitting using this expression for a single fluorescent species with background effectively combines the information from moment analysis (33) with the information from FCS with dark states included (31).

The background count rate k_{bkgd} for each concentration was determined from Cph1 solutions in the absence of the fluorescent mutant PR1. The brightness q reflects the average photon count rate of the fluorescent molecule, and c is the occupancy, which describes how frequently the photon count rate is above the background signal. All other parameters are the same as in the correlation equations. The resulting brightness is a convolution of the fluorescence quantum yield of the individual proteins, the dark-state conversion, and any other competing processes. The fluorescent dyes Atto 655, Alexa Fluor 660, and Cy5.18 were analyzed by using the covariance equation with $T = 0$, which effectively removes the dark-state term, because the dyes show essentially no dark-state interconversion.

This work was supported by National Institutes of Health Grant GM068552-01 (to J.C.L.), National Science Foundation Center for Biophotonics Science and Technology Grant PHY-0120999, the Experimental Physical Chemistry Division of the National Science Foundation, the University of California, Davis, Biotechnology Training Program, and a Lawrence Livermore National Laboratory Student Employee Graduate Research Fellowship (to A.E.M.). Work at Lawrence Livermore National Laboratory was performed under the auspices of the U.S. Department of Energy by University of California Lawrence Livermore National Laboratory under Contract W-7405-Eng-48.

1. Sage, L. C. (1992) *Pigment of the Imagination: A History of Phytochrome Research* (Academic, San Diego).
2. Franklin, K. A. & Whitelam, G. C. (2005) *Ann. Bot. (London)* **96,** 169–175.
3. Montgomery, B. L. & Lagarias, J. C. (2002) *Trends Plant Sci.* **7,** 357–366.
4. Karniol, B. & Vierstra, R. D. (2005) in *Photomorphogenesis in Plants and Bacteria: Function and Signal Transduction Mechanism*, eds. Schäfer, E. & Nagy, F. (Springer, Dordrecht, The Netherlands), 3rd Ed., 65–98.
5. Nagy, F. & Schäfer, E. (2002) *Annu. Rev. Plant Biol.* **53,** 329–355.
6. Chen, M., Chory, J. & Fankhauser, C. (2004) *Annu. Rev. Genet.* **38,** 87–117.
7. Huq, E. & Quail, P. H. (2005) in *Handbook of Photosensory Receptors*, eds. Briggs, W. R. & Spudich, J. A. (Wiley–VCH, Weinheim, Germany), pp. 151–170.
8. Rockwell, N. C., Su, Y. S. & Lagarias, J. C. (2006) *Annu. Rev. Plant Biol.* **57,** 837–858.
9. Braslavsky, S. E. (2003) in *Photochromism: Molecules and Systems*, eds. Dürr, H. & Bouas-Laurent, H. (Elsevier Science, Amsterdam), pp. 738–755.
10. Glazer, A. N. (1999) in *Chemicals from Microalgae*, ed. Cohen, Z. (Taylor & Francis, London), pp. 261–280.
11. Murphy, J. T. & Lagarias, J. C. (1997) *Curr. Biol.* **7,** 870–876.
12. Fischer, A. J. & Lagarias, J. C. (2004) *Proc. Natl. Acad. Sci. USA* **101,** 17334–17339.
13. Fischer, A. J., Rockwell, N. C., Jang, A. Y., Ernst, L. A., Waggoner, A. S., Duan, Y., Lei, H. & Lagarias, J. C. (2005) *Biochemistry* **44,** 15203–15215.
14. Bose, G., Schwille, P. & Lamparter, T. (2004) *Biophys. J.* **87,** 2013–2021.
15. Elson, E. L. & Magde, D. (1974) *Biopolymers* **13,** 1–27.
16. Haupts, U., Maiti, S., Schwille, P. & Webb, W. W. (1998) *Proc. Natl. Acad. Sci. USA* **95,** 13573–13578.
17. Gambetta, G. A. & Lagarias, J. C. (2001) *Proc. Natl. Acad. Sci. USA* **98,** 10566–10571.
18. Park, C. M., Shim, J. Y., Yang, S. S., Kang, J. G., Kim, J. I., Luka, Z. & Song, P. S. (2000) *Biochemistry* **39,** 6349–6356.
19. Lamparter, T., Esteban, B. & Hughes, J. (2001) *Eur. J. Biochem.* **268,** 4720–4730.
20. Strauss, H. M., Schmieder, P. & Hughes, J. (2005) *FEBS Lett.* **579,** 3970–3974.
21. Park, C. M., Kim, J. I., Yang, S. S., Kang, J. G., Kang, J. H., Shim, J. Y., Chung, Y. H., Park, Y. M. & Song, P. S. (2000) *Biochemistry* **39,** 10840–10847.
22. Vaiana, A. C., Neuweiler, H., Schulz, A., Wolfrum, J., Sauer, M. & Smith, J. C. (2003) *J. Am. Chem. Soc.* **125,** 14564–14572.
23. Marme, N., Knemeyer, J. P., Sauer, M. & Wolfrum, J. (2003) *Bioconjug. Chem.* **14,** 1133–1139.
24. Wagner, J. R., Brunzelle, J. S., Forest, K. T. & Vierstra, R. D. (2005) *Nature* **438,** 325–331.
25. Tsien, R. Y. (1998) *Annu. Rev. Biochem.* **67,** 509–544.
26. Shimizu-Sato, S., Huq, E., Tepperman, J. M. & Quail, P. H. (2002) *Nat. Biotechnol.* **20,** 1041–1044.
27. Levskaya, A., Chevalier, A. A., Tabor, J. J., Simpson, Z. B., Lavery, L. A., Levy, M., Davidson, E. A., Scouras, A., Ellington, A. D., Marcotte, E. M. & Voigt, C. A. (2005) *Nature* **438,** 441–442.
28. Laurence, T. A., Fore, S. & Huser, T. (2006) *Opt. Lett.* **31,** 829–831.
29. Rigler, R., Mets, U., Widengren, J. & Kask, P. (1993) *Eur. Biophys. J.* **22,** 169–175.
30. Schwille, P. (2001) *Cell Biochem. Biophys.* **34,** 383–408.
31. Widengren, J., Mets, U. & Rigler, R. (1995) *J. Phys. Chem.* **99,** 13368–13379.
32. Masuda, A., Ushida, K. & Okamoto, T. (2005) *Biophys. J.* **88,** 3584–3591.
33. Qian, H. & Elson, E. L. (1990) *Proc. Natl. Acad. Sci. USA* **87,** 5479–5483.